

RSC Advances



This is an *Accepted Manuscript*, which has been through the Royal Society of Chemistry peer review process and has been accepted for publication.

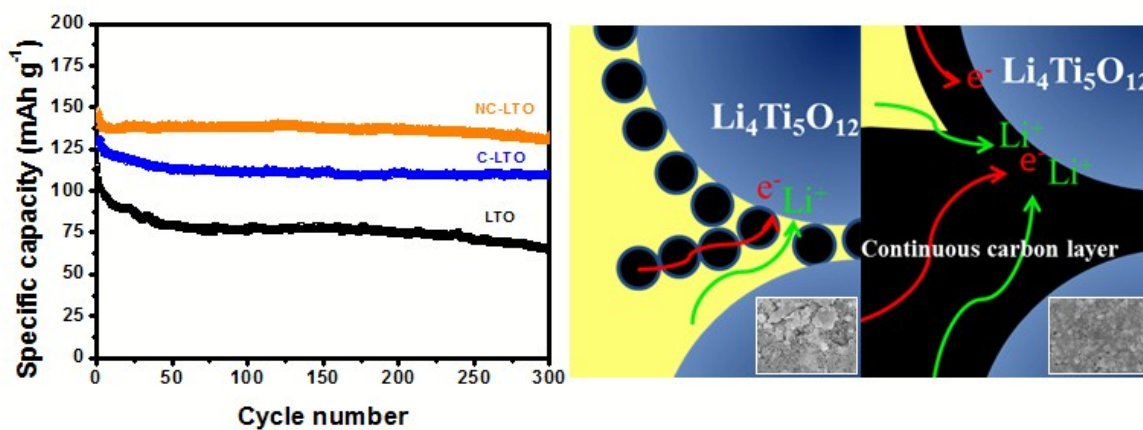
Accepted Manuscripts are published online shortly after acceptance, before technical editing, formatting and proof reading. Using this free service, authors can make their results available to the community, in citable form, before we publish the edited article. This *Accepted Manuscript* will be replaced by the edited, formatted and paginated article as soon as this is available.

You can find more information about *Accepted Manuscripts* in the [Information for Authors](#).

Please note that technical editing may introduce minor changes to the text and/or graphics, which may alter content. The journal's standard [Terms & Conditions](#) and the [Ethical guidelines](#) still apply. In no event shall the Royal Society of Chemistry be held responsible for any errors or omissions in this *Accepted Manuscript* or any consequences arising from the use of any information it contains.

Graphical abstract

Improvement of the Ar/N₂ binary plasma-treated carbon passivation layer deposited on Li₄Ti₅O₁₂ electrodes for stable high-rate lithium ion battery



KEYWORDS: lithium titanate; passivation layer; atmospheric pressure plasma; solid electrolyte interphase; lithium ion batteries

Improvement of the Ar/N₂ binary plasma-treated carbon passivation layer deposited on Li₄Ti₅O₁₂ electrodes for stable high-rate lithium ion battery

Chun-Kai Lan^a, Chun-Chi Chang^a, Cheng-Yu Wu^a, Bing-Hong Chen^a and Jenq-Gong Duh^{a*}

^aDepartment of Materials Science and Engineering, National Tsing Hua University, Hsinchu, Taiwan 30010

*Corresponding author:

Tel.: 886-3-5712686

Fax: 886-3-5712686;

E-mail: jgd@mx.nthu.edu.tw (Jenq-Gong Duh)

Abstract

In this study, nanoscale carbon overlayers, with and without nitrogen doping, have been investigated as surface passivation layers to enhance the rate capability and cycling stability of $\text{Li}_4\text{Ti}_5\text{O}_{12}$ (LTO). As indicated by optical emission spectroscopy, Raman spectra and high resolution X-ray photoelectron spectroscopy analysis, the nitrogen successfully dopes into the carbon overlayer by Ar/ N_2 binary plasma irradiation, owing to the interaction between the carbon overlayer and chemically reactive plasma species such as N_2^+ and N. In addition, the results of SEM and XPS depth profiles also prove that the N-doped carbon overlayer can effectively suppress the formation of a resistive solid-electrolyte-interface (SEI) film. The electrochemical test results demonstrate that the LTO coated with N-doped carbon overlayer (NC-overlayer/LTO) exhibits a superior capacity (133 mAh g^{-1}) and excellent stability with 91% capacity retention over 300 cycles under a high C rate (10 C). The excellent electrochemical performance of NC-overlayer/LTO can be attributed to the N-doped carbon passivation layer that effectively facilitates Li^+ ion diffusion and reduces internal resistance.

1. Introduction

Lithium ion batteries (LIBs), as the key technology in electrical energy storage systems, are applied in a wide range of applications for modern portable electronic devices because of their high energy density, long lifespan, high operating voltage and absence of memory effects, as compared to the other type of batteries like Ni-Cd, Ni-MH and lead acid batteries.¹ Spinel lithium titanate ($\text{Li}_4\text{Ti}_5\text{O}_{12}$, LTO) with a theoretical capacity of 175 mAh g^{-1} has been regarded as a highly promising anode materials candidate for commercialized graphite because of its inherent advantages. Lithium titanate-based materials exhibit a relatively higher and more stable working voltage (1.55 V vs. Li^+/Li), effectively preventing the growth of lithium dendritic on the electrode surface during the charge-discharge process.²⁻⁶ The negligible volume expansion during lithium intercalation/deintercalation process also guarantees excellent safety and long-term cycling stability over graphite and other metallic oxides like SnO_2 or Fe_3O_4 . It is also well-known that the formation of solid electrolyte interphase (SEI) films is usually below 1 V, and such layers are considered as main factors to cause active lithium ion loss and increase the internal impedance of cells. This is another important reason to tout $\text{Li}_4\text{Ti}_5\text{O}_{12}$ as a potential anode material for high power Li-ion batteries.

However, He et al. recently reported that solid electrolyte interphase compounds could also be detected even on the surfaces of electrodes operating at above 1 V, and such resistive layers could greatly affect the capacity retention and rate capability of LTO.⁷ Furthermore, rate performance of $\text{Li}_4\text{Ti}_5\text{O}_{12}$ was also handicapped by sluggish lithium diffusion and its insulated character, owing to empty Ti 3d orbital ($\sigma_e = 10^{-9} \sim 10^{-13} \text{ S/cm}$; $\sigma_{\text{Li}} = 10^{-7} \sim 10^{-9} \text{ S/cm}$). Therefore, numerous efforts have been devoted to improve the electronic conductivity of $\text{Li}_4\text{Ti}_5\text{O}_{12}$ -based anode materials, including coating $\text{Li}_4\text{Ti}_5\text{O}_{12}$ with conductive species (e.g., TiN, Au, carbon),⁸⁻¹⁰

synthesizing nanostructured materials with various morphologies (nanoparticles, nanofibers, nanosheets and mesoporous),¹¹⁻¹⁵ or doping foreign elements (e.g., Cr, Al, Nb, Ni, Mn, La, Ru, F, Br or N) into L, Ti, or O sites.¹⁶⁻²² Unfortunately, most of them merely serve a single function and have almost no direct effect on SEI formation. Despite a few studies which were conducted to investigate the reactivity between lithium titanate and electrolytes in the past, little attention has been paid to effectively inhibit the irreversible interfacial reaction and improve electrochemical performance at the same time.

Recently, Park et al. reported that the deposition of metal fluoride on a LiCoO₂ cathode exhibited excellent capacity retention without apparent loss in the first 50 cycles.²³ Yesibolati et al. also improved the cycling stability of their batteries by coating nanoscale HfO₂ layers on SnO₂/reduced graphite oxide electrodes.²⁴ The construction of a robust passivation layer between electrolyte and electrode could be a promising method to effectively mitigate the irreversible side reaction between the electrolyte and the active material and afford better performance. Although this method has been widely applied in several electrode materials systems, to our best knowledge, the effect of passivation layer coating on Li₄Ti₅O₁₂-based anode materials has never been systematically investigated. Zhu et al. also reported that carbon layer with appropriate content defects not only improve electronic conductivity, but allow Li-ion pass through to react with Li₄Ti₅O₁₂ bulk.

Herein, we report for the first time on the direct coating of nanoscale carbon overlayers on electrode surfaces, the aim of which was to realize the excellent chemical performance of Li₄Ti₅O₁₂-based anodes, based on the concept of designing a conducting passivation layer, as illustrated in Fig. 1 (a). Atmospheric pressure plasma, generated by radio frequency electromagnetic radiations at ambient pressure (~0.101MPa), successfully improves its

uniformity by avoiding arcing and eliminated the expensive vacuum apparatus, resulting in a fast development in a wide range of applications such as surface coating, air-pollution control and biomedical sterilization. Particularly, in the field of surface modification, APPs also have attracted growing attention over the last two decade owing to its capability to tailor the surface properties and to functionalize surfaces in a non-thermal and cost-effective pathway. More significantly, APPs could be easily incorporated into other fabrication processes as compared to other traditional techniques. Therefore, Ar/ N₂ binary APPs jet, a facile and eco-friendly device, was set up as the nitrogen doping source to tune the electronic properties of carbon overlayer. All results demonstrated that the deposition of an N-doped carbon overlayer significantly promoted an excellent rate performance of lithium titanate and effectively alleviated the parasitic reaction between electrolyte and electrode. Furthermore, the effects of a carbon-overlayer coating on lithium ion diffusivity and internal resistance were examined in detail by electrochemical impedance spectroscopy.

2. Experimental section

Material preparation: The chemicals used in the study were anhydrous lithium chloride (LiCl, 99%, Alfa Aesar), titanium (IV) chloride (TiCl₄, >98.0%, Fluka), and oxalic acid dihydrate (H₂C₂O₄·2H₂O, >99.5%, Sigma-Aldrich). Following typical methods for this kind of procedure, appropriate amounts of anhydrous lithium chloride, titanium (IV) chloride and 70 wt% oxalic acid dihydrate were fully mixed at 200°C for reacting 0.5 h, and then slurry-like Li-Ti-O oxalate was sintered at 400 °C for 3 h and calcined at 800 °C for 10 h in air to obtain Li₄Ti₅O₁₂ powders.

Characterization: Optical emission spectroscopy analyzed the main plasma species in the Ar/N₂ plasma and spectroscopic measurements in the spectral range of 250–450 nm were obtained from a USB2000 Miniature Fiber Optic Spectrometer (Ocean Optics, USA). The

resolving power of the USB2000 Miniature Fiber Optic Spectrometer was 0.3 nm. The crystalline phase of the prepared electrodes were characterized on an X-ray diffractometer (Rigaku, TTRAXIII, Japan) using Cu K α radiation ($\lambda=1.5406$ Å) at 50 kV and 300 mA in grazing incident (GI) mode. During GI-XRD measurements, all diffractograms were recorded from 10° to 80° [2theta] in steps of 0.05° at a scan speed of 2°min⁻¹. The incident angle was fixed at 0.5°. A field emission scanning electron microscope (JEOL, FE-7600, Japan) was employed to examine the surface morphology of all samples. Raman spectra of all samples were obtained using a HR800-UV Micro-Raman Spectrometer (HORIBA Jobin Yvon, Japan) with a 514.5 nm laser source. The presence of N and depth profile analysis were measured by high-resolution X-ray photoelectron spectroscopy (HR XPS) analysis conducted on a ULVAC-PHI Quantera SXM system. Fourier-transform infrared (FT-IR) spectra were measured using a Bruker Tensor 27 IR Spectrometer.

Electrode fabrication: Pristine LTO electrodes used for electrochemical examinations were fabricated by mixing active material powders with conductive carbon (super P) and binder (PVDF) at a weight ratio of 80:13:7 in N-methyl-2-pyrrolidinone (NMP) solvent. The electrode sheet was prepared by casting the slurry in a piece of Cu foil and drying at 100 °C under vacuum for 12 h. Then, a carbon overlayer with appropriate thickness was fabricated onto Li₄Ti₅O₁₂ based cathode plates using a DC magnetron sputtering system with 1.3×10^{-4} Pa base pressure and 4.5×10^{-1} Pa working pressure. The sputtering was performed at 80 W (DC power, ADVANCED ENERGY-MDX 500) with a pure carbon target (2-in. in diameter). Subsequently, the as-deposited LTO electrodes were exposed to the Ar/N₂ plasma jet (APPJs) irradiation with an electric power of 30 W for 5 minutes. The CR2032 coin-type half cells were assembled with Li metal as the counter electrode, porous polypropylene film as the separator, and 1 M LiPF₆ in

EC/DMC (v:v=1:1) as the electrolyte in an argon-filled glove box. For an easy discussion, the carbon overlayer-coated electrodes and the plasma-treated electrodes are referred to as C-overlayer/LTO and NC-overlayer/LTO, respectively.

Electrochemical performance: Electrochemical tests were performed by using two-electrodes of 2032 type coin cells (20 mm in diameter and 3.2 mm thick). The C rate capability and cycling stability test were performed between 2.5 and 1.0 V at different C rates (1C = 175 mAh g⁻¹) vs. Li/Li⁺ on an electrochemical multi-channel tester (BT-2000, Arbin, USA). The electrochemical impedance spectra (EIS) were conducted on an electrochemical workstation (Ametek 263A, USA). The EIS measurements were carried out after the first cycle and maintained under a stable voltage of 1.60 V (vs. Li/Li⁺) for a long period of time at the delithiated state. Then, EIS were operated by applying an AC voltage of 10mV amplitude over a frequency ranging from 100 kHz to 10 mHz at a constant voltage of 1.60 V (vs. Li/Li⁺).

3. Results and discussion

In order to investigate the influence of carbon overlayer coating and plasma irradiation on the phase composition of LTO, the XRD on grazing-incident mode, which was more sensitive to slight changes of superficial particles than wide-angle mode, was chosen to examine all the samples. As shown in Fig. 3, the XRD patterns of pristine LTO, C-overlayer/LTO and NC-overlayer/LTO could be indexed as spinel cubic structures with Fd3m groups according to the JCPDS card No.26-1198. No obvious impurities were detected from diffraction patterns, indicating that the sputter process and APPs plasma treatment didn't induce other phase formations. Furthermore, there were no diffraction peaks corresponding to carbon owing to the domination of an amorphous structure. LTO, C-overlayer/LTO and NC-overlayer/LTO were

further characterized by Raman spectroscopy to derive information about structure variation after the sputter process and APPs plasma treatment. For pristine LTO (Fig. 4 (a)), five Raman-active vibration bands were observed at 230, 270, 349, 422 and 674 cm^{-1} , respectively, in good agreement with the features of spinel structure $A[B_2]O_4$, which has five active Raman modes: 3 F_{2g} , E_g and A_{1g} .^{25,26} The Raman spectrums of C-overlayer/LTO and NC-overlayer/LTO were also characterized as spinel structures, while the intensity of peaks were slightly broader and weaker compared with pristine LTO, implying that the structure of lithium titanate became disordered during carbon passivation layer deposition. These could be attributed to the direct bombardment between high-energy species and the electrode surface during the sputter process, causing the formation of defects in the $Li_4Ti_5O_{12}$ crystalline structure. This disordered structure of lithium titanate could result in facilitation of Li ion transfer in C-overlayer/LTO and NC-overlayer/LTO.

The presence of carbon is also confirmed by two bands around 1594 cm^{-1} and 1356 cm^{-1} , as shown in Fig 4 (b). The intense band at 1594 cm^{-1} is attributed to G-band vibration originating from well-ordered hexagonal graphitic carbon structures, and the other band at 1356 cm^{-1} is attributed to a D-band of disordered structure carbon.²⁷ Furthermore, the D/G ratio (I_D/I_G) serves as an important structural value to determine the quality of carbon. Graphitic carbon exhibits high electron conductivity, yet its compact layered structure may block lithium diffusion. On the other hand, amorphous carbon is beneficial for lithium to pass through due to defects or cracks, however such benefits may be somewhat negated by the poorer electron conductivity.²⁸ The measured carbon signal of pristine LTO could be attributed to the existence of carbon black in the electrodes, but it is more noteworthy that the NC-overlayer/LTO demonstrated a higher I_D/I_G ratio of 0.96 than that of C-overlayer/LTO (0.91), indicating the carbon overlayer exhibited more disorder phase than graphitic phase after Ar/ N_2 plasma treatment. Apparently, Ar and N_2 reactive

plasma species' bombardment effects deteriorated the crystalline carbon forms. In consideration of such ratios of carbon structures, a plasma-treated (NC-overlayer/LTO) carbon overlayer could offer a conductive network as well as an unimpeded lithium diffusion channel.

Because the Ar/ N₂ binary APPs jet is used to introduce nitrogen into carbon overlayer, the investigation of energetic species in plasma will facilitate the subsequent discussion of surface chemical states. To diagnose the plasma phase, the optical emission spectrum (OES) as a non-invasive and in-situ method, was applied to analyze all the energetic species emitted from a Ar/N₂ plasma jet during the irradiation process. It is attempted to discuss the formation mechanisms of Ar^{*}, N₂⁺, N₂^{*} and N species in the discharge gas. As shown in Fig. 2, a number of argon emission lines can be observed in the spectra, indicating that argon ion species with various energy levels exist inside the plasma. Among these characteristic peaks, the metastable states of 11.55eV (4s 3P₂) and 11.72 eV (4s 3P₀) for argon atoms were often considered to be produced from the ground state by electronic excitation:



The other two characteristic molecules, N₂^{*} (second positive system) and N₂⁺ (first negative system), were also detected around 337.1 nm and 384 nm, respectively.²⁹ The N₂^{*} emission lines mainly consisted of the radiative state (C³Π_u → B³Π_g) and the metastable state (B³Π_u⁺ → A³Σ_u⁺). Regarding the radiative state, there are two major formation processes, namely, the first one comes about from impact by energetic electrons with energies above 6.1 eV. The second one comes from an internal energy transfer from metastable state argon atoms (11.55eV and 11.72 eV), which is higher than the minimum excited energy of nitrogen molecules (11.1 eV), to ground state nitrogen molecules. In addition, the singly-ionized N₂⁺ excited state could be populated from the ground state of nitrogen molecules either by electron impact excitation

(>15.5eV) or reactions between Ar* metastable molecules by Pinning ionization,³⁰ which is produced by the following process:



Then, the main atomic N species might be generated from the dissociation of N₂⁺ by electron impact via³¹



XPS analysis was performed to determine the surface chemical states and results are displayed in Fig 5. As shown in Fig 5 (a), LTO, C-overlayer/LTO and NC-overlayer/LTO revealed typical XPS wide spectra, however, the Ti 2p peaks of C-overlayer/LTO and NC-overlayer/LTO were difficult to observe in XPS spectra, as compared to that of the pristine LTO sample. These could be explained by the thickness of carbon overlayer (~40 nm) coated over the electrodes beyond the probing depth of the X-ray beam (5~10nm), and the received image of the electrodes became weakened. The high resolution N 1S core-level spectrum, as revealed in Fig. 5 (b), could be deconvoluted into three peaks to investigate various configurations of nitrogen-containing functional groups in the N-doped carbon overlayer. The peaks at binding energies of 398.2, 400.1 and 401.6 eV can be correlated to different doping sites in the graphic carbon structure, that is, pyridinic, pyrrolic and quaternary N atoms, respectively, as shown in Fig. 5 (c).³² These are explained by the fact that the N₂⁺, N₂^{*} and Ar* excite the carbon overlayer surface and break C-C bonding, creating excited sites followed by reaction with the atomic nitrogen species (N) in the discharge gas.³³ In general, the appearance of pyridinic and pyrrolic N atoms could not only contribute electrons in the π-system to enhance the overall electric conductivity, but also facilitate the diffusion of lithium ions in carbon layer.³⁴

The rate performance of pristine LTO, C-overlayer/LTO and NC-overlayer/LTO was compared in Fig. 6 (a). The C-overlayer/LTO and NC-overlayer/LTO delivered a capacity around 174-177 mAh g⁻¹ at 0.5 C, which was close to the theoretical capacity, while that of pristine LTO was 150 mAh g⁻¹. The capacity of pristine LTO was merely 105 and then 79 mAh g⁻¹ as the discharge rate was increased from 5 to 10C, respectively. On the other hand, NC-overlayer/LTO and C-overlayer/LTO exhibited superior high capacities of 134 and 121 mAh g⁻¹ at 10 C, respectively. Consequently, NC-overlayer/LTO and C-overlayer/LTO at 10 C could retain 78 % and 70%, respectively, of cell capacity at 1 C, much higher than uncoated LTO (54 %). This result suggests that the carbon overlayer can effectively enhance the rate performance of Li₄Ti₅O₁₂ via a continuous conductive network, as illustrated in Fig. 1 (b). In addition, at a relatively low C-rate, i.e. 1 C, a similar capacity around 170 mAh g⁻¹ was achieved by NC-overlayer/LTO and C-overlayer/LTO, whereas NC-overlayer/LTO demonstrated a higher reversible capacity at 10 C than C-overlayer/LTO, indicating that a better rate capability was indeed accomplished by the N-doped carbon overlayer.

Fig. 6 (b) and (c) demonstrate the cycling performance and corresponding coulombic efficiency of coin cells derived from LTO, C-overlayer/LTO and NC-overlayer/LTO at the charge/discharge rate of 10 C for 300 cycles. All the samples showed fairly good cycling stability due to the unique zero strain character of Li₄Ti₅O₁₂ during the Li⁺ insertion-extraction process. After the 300th cycle, the capacity for the sample coated N-doped carbon overlayer still maintained the competitive value of 133 mA g⁻¹ with 91% capacity retention, which is a better rate as compared with other N-doped carbon-coated Li₄Ti₅O₁₂ electrodes fabricated via chemical methods.³⁵⁻³⁷ Furthermore, the large capacity decay of the pristine LTO was also observed during initial cycles. This might be correlated to the reaction between lithium titanate particles and

electrolytes, resulting in irreversible capacity loss by the formation of a solid electrolyte interface (SEI).^{38,39} Fig 6 (d) presents the cyclic voltammetry (CV) profile of all samples scanned at 0.1 mV S⁻¹ between 2.5 and 1.0V. A pair of well-defined redox peaks was observed around 1.66/1.5V, which were characteristic of Li⁺ insertion/deinsertion in Li₄Ti₅O₁₂ materials.³ The values of potential separation between the anodic and cathodic peaks for all samples are listed in Table 1. Clearly, NC-overlayer/LTO exhibited smaller potential separation values than those of other samples, which also suggests it has faster electrons and better ionic conductivity.

Fig. 7 represents the typical top surfaces of LTO, C-overlayer/LTO and NC-overlayer/LTO samples before and after 10 cycles at 0.1C. As shown in Fig. 7 (a), the LTO sample exhibited a porous structure before cycling, and the lithium titanate particles were directly exposed to the surface of the electrodes. The C-overlayer/LTO and NC-overlayer/LTO showed relatively dense and smooth surface morphology due to the coverage of the carbon passivation layer. Interestingly, even after the plasma irradiation process, it is difficult to distinguish the difference in surface morphology between C-overlayer/LTO and NC-overlayer/LTO, implying that Apps treatment could be viewed as a non-destructive doping method. After cycling, a thick and smooth SEI layer was built upon on the pristine LTO electrodes. However, despite the formation of an SEI layer, the C-overlayer/LTO and NC-overlayer/LTO electrodes displayed porous structure, ensuring electrolyte pathways (Fig. 7 (e) and (f)). This interesting difference could be associated with the presence of the carbon overlayer. The carbon overlayer, serving as a passivation layer, effectively reduced the contact area between nonaqueous electrolytes and the lithium titanate, which in turn decrease the reactivity of electrolytes. XPS depth profiles were used to further investigate all samples as depicted in Fig. 8. The interface between the carbon layer and the LTO electrode is determined by the intensity ratio between Ti and O (5:12), and the position of the

carbon layer is confirmed by the maximum value of the C 1s signal. As shown in Fig. 8 (a), the depth of SEI film for the pristine LTO case corresponds to the depth of the 3 min sputter time, while that for C-overlayer/LTO and NC-overlayer/LTO is merely 2 and 1 min, respectively. This also supports the above SEM result that a carbon layer could effectively suppress the formation of an SEI film.

Furthermore, to identify the composition of the SEI film for all samples, FTIR analysis was conducted to analyze the surface of all samples. As shown in Fig. 9, main peaks at 1416, 1503 and 1634 cm^{-1} indicated that the main reaction products upon the electrode surface are Li_2CO_3 , ROCOOLi .⁴⁰ The presence of Li organic carbonates and Li_2CO_3 , stemming from the decomposition of electrolyte solvents, also supports the above-cited viewpoint that electrolytes will be reduced at $\text{Li}_4\text{Ti}_5\text{O}_{12}$ electrodes even operating at voltages above 1 V. This means that all three samples form a resistive layer.

Electrochemical impedance spectra (EIS) was performed to get further insight about all samples' kinetic behavior as shown in Fig. 10. The coin cell, after cycling for 3 times at 0.1C, was kept at 1.6 V and measured via the application of an oscillating voltage of 10 mV amplitude over a frequency ranging from 10 mHz to 100 kHz. For all electrodes, the EIS spectra consisted of one depressed semicircle from the high to intermediate frequency region followed by a straight-line portion in the range of medium-to-low frequency. The Nyquist plots were fitted by ZView software and the equivalent circuit is shown in the inset of Fig. 10 (a).^{41,42} In the equivalent circuit, R_s the high frequency indicates that the bulk electrolyte resistance and R_{SEI} is associated with a thin layer of compound formed on the electrode/electrolyte interface. The interception of the depressed semicircle at Z_{re} axis in the medium frequency region corresponds

to charge transfer resistance (R_{ct}). The sloped line in low frequency is associated with Warburg impedance (W). The values of resistance parameters used in the circuit are listed in Table 2.

It is evident that charge-transfer resistance of the carbon overlayer coated samples was much lower than the pristine one, indicating a faster charge transfer reaction at the active materials interface. This could be attributed to the continuous thin layer of carbon situated between primary particles, providing an effective pathway to conduct electrons within carbon coated samples. Furthermore, the decomposability of electrolyte generally depended on the situation of the active material surface. The deposition of a continuous carbon layer, acting as a passivation layer between electrolyte and electrode materials, successfully suppressed the formation of SEI, leading to a smaller R_{SEI} value. It is worth noting that the NC-overlayer/LTO demonstrated the smallest values of R_{SEI} and R_{ct} among all samples. This could be ascribed to the presence of defects like pyridinic, pyrrolic and quarternary N atoms, effectively improving the electronic conductivity and charge transfer reaction in the interface.^{47,48} Furthermore, the reaction between those nitrogen incorporations and electrolytes could provide a thinner SEI film and LiN_x species on the electrode surface to facilitate interfacial reactions.⁴³

Furthermore, the lithium diffusion coefficient of lithium ions in the bulk electrode was calculated according to the assumption that semi-finite diffusion via Eq. 5.⁴⁴⁻⁴⁶

$$D = \frac{R^2 T^2}{2A^2 n^4 F^4 C^2 \sigma^2} \quad (5)$$

where ω : the angular frequency, D : the diffusion coefficient, R : the gas constant (8.314 kJ mol⁻¹), T : the absolute temperature (300 K), F : Faraday's constant (96500 C mol⁻¹), A : the apparent area of the electrode (1.37 cm²), C : the molar concentration of Li⁺ ions, $L1$: conductance of coaxial cable and σ : the Warburg impedance coefficient. The relationship between real impedance (Z_{re}) and angular frequency in the low frequency region is described by

Eq. 6. and shown in Fig. 10 (b). The values of the lithium diffusion coefficient are listed in Table 2.

$$Z_{re} = R_s + R_{ct} + \sigma\omega^{-1/2} \quad (6)$$

It was demonstrated that NC-overlayer/LTO showed the highest D_{Li} value ($1.47 \times 10^{-8} \text{ cm}^2 \text{ s}^{-1}$) over that of pristine LTO ($1.76 \times 10^{-9} \text{ cm}^2 \text{ s}^{-1}$) and C-overlayer/LTO ($1.25 \times 10^{-8} \text{ cm}^2 \text{ s}^{-1}$). This result also confirms that the N-doped carbon overlayer is more beneficial to lithium diffusion, which is also in agreement with the previous discussion.

In short, the kinetics of both electrons and lithium are facilitated through the introduction of a carbon overlayer combined with Ar/N₂ plasma treatment. This is because the lithium diffusion rate of NC-overlayer/LTO is higher than that of pristine LTO or C-overlayer/LTO. Both the thinner SEI layer and N atoms defecting the formation of the carbon layer contribute to this higher diffusion rate and lower charge-transfer resistance. This results in favorable rate capability in NC-overlayer/LTO.

4. Conclusions

This study demonstrates that N-doped carbon and carbon passivation layers deposited onto LTO electrodes might prevent the active materials surface from irreversible reactions and construct continuous electronic pathways. Nitrogen was successfully doped into the carbon overlayer through Ar/N₂ plasma irradiation at atmospheric pressure. The presence of nitrogen incorporations in the carbon layer could provide extra electrons and lower Li⁺ diffusion barriers. Meanwhile, the thickness of the solid-electrolyte-interphase film was significantly reduced. In summary, NC-overlayer/LTO exhibited a desirable electrochemical performance for energy

storage application. Through the utilization of a passivation layer, the N-doped carbon overlayer-coated LTO could be the potential anode material for high-rate lithium ion batteries.

ACKNOWLEDGMENT

This study was financially supported by Ministry of Science and Technology, under project No. NSC 102-2622-E-007-017-CC1.

References

- (1) B. Dunn, H. Kamath and J.M. Tarascon, *Science*, 2011, 334, 928-935.
- (2) V. R. Subramanian, P. Yu, B.N. Popov and R. E. White, *J. Power Sources*, 2001, 96, 396-405.
- (3) T. Ohzuku, A. Ueda and N. Yamamoto, *J. Electrochem. Soc.*, 1995, 142, 1431-1435.
- (4) J. Wolfenstine and J. L. Allen, *J. Power Sources*, 2008, 180, 582-585.
- (5) T.F. Yi, Y. Xie, Y.R. Zhu, R.S. Zhu and H. Shen, *J. Power Sources*, 2013, 222, 448-454.
- (6) T.F. Yi, S.Y. Yang and Y. Xie, *J. Mater. Chem. A*, 2015, 3, 5750-5777.
- (7) Y.B. He, B. Li, M. Liu, C. Zhang, W. Lv, C. Yang, J. Li, H. Du, B. Zhang, Q.H. Yang, J.K. Kim and F. Kang, *Sci. Rep.*, 2012 2, 913-921.
- (8) Y. Ren, P. Lu, X. Huang, J. Ding, H. Wang, S. Zhou, Y. Chen and B. Liu, *RSC Adv.*, 2015, 5, 55994-56000.
- (9) J. Liu, Y. Shen, L. Chen, Y. Wang and Y. Xia, *Electrochim. Acta*, 2015, 156, 38-44.
- (10) H. Park, T. Song, H. Han and U. Paik, *J. Power Sources*, 2013, 244, 726-730.

- (11) J. Liu, K. Song, P. A. van Aken, J. Maier and Y. Yu, *Nano Lett.* 2014, 14, 2597–2603.
- (12) T.F. Yi, Z.K. Fang, Y. Xie, Y.R. Zhu and S.Y. Yang, *ACS Appl. Mater. Interfaces* 2014, 6, 20205–20213.
- (13) S.L. Chou, J.Z. Wang, H.K. Liu and S.X. Dou, *J. Phys. Chem. C* 2011, 115, 16220–16227.
- (14) S. Deng, J. Li, S. Sun, H. Wang, J. Liu and H. Yan, *Electrochimi. Acta*, 2014, 146, 37-43.
- (15) E. Kang, Y. S. Jung, G.H. Kim, J. Chun, U. Wiesner, A. C. Dillon, J. K. Kim and J. Lee, *Adv. Funct. Mater.* 2011, 21, 4349–4357.
- (16) Z. Wang, G. Chen, J. Xu, Z. Lv and W. Yang, *J. Phys. Chem. Solids*, 2011, 72, 773- 778.
- (17) T.F. Yi, Y. Xie, L.J. Jiang, J. Shu, C.B. Yue, A.N. Zhou and M.F. Ye, *RSC Adv.*, 2012, 2, 3541–3547.
- (18) T.F. Yi, Y. Xie, Q.J. Wu, H.P. Liu, L.J. Jiang, M.F. Ye and R.S. Zhu, *J. Power Sources*, 2012, 214, 220-226.
- (19) B. Tian, H. Xiang, L. Zhang, Z. Li, H. Wang, *Electrochimi. Acta*, 2010, 55, 5453- 5458.
- (20) Y.R. Jhan and J.G. Duh, *Electrochimi. Acta*, 2012, 63, 9- 15.
- (21) Y. Ma, B. Ding, G. Ji and J.Y. Lee, *ACS Nano*, 2013, 12, 10870–10878.
- (22) C.K. Lan, S.I. Chuang, Q. Bao, Y.T. Liao, J.G. Duh, *J. Power Sources*, 2015, 275, 660-667.
- (23) J.S. Park, A. U. Mane, J.W. Elam and J.R. Croy, *Chem. Mater.* 2015, 27, 1917–1920.

- (24) N. Yesibolati, M. Shahid, Wei. Chen, M. N. Hedhili, M. C. Reuter, F. M. Ross and H. N. Alshareef, *Small* 2014, 10, 2849–2858.
- (25) Y. Tang, F. Huang, W. Zhao, Z. Liu and D. Wan, *J. Mater. Chem.*, 2012, 22, 11257-11260.
- (26) N.C. Saha and H.G. Tompkins, *J. Appl. Phys.*, 1992, 72, 3072- 3079.
- (27) C. Thomsen and S. Reich, *Phys. Rev. Lett.* , 2000, 85, 5214
- (28) T. Yuan, R. Cai and Z. Shao, *J. Phys. Chem. C*, 2011, 115, 4943–4952.
- (29) S A. Qayyum, S. Zeb, M.A. Naveed, N.U. Rehman, S.A. Ghauri and M. Zakauallah, *J. Quant. Spectrosc. Radiat. Transfer*, **2007**, 107, 361–371.
- (30) S. Bockel, J. Amorim, G. Baravian, A. Ricard and P. A. Stratil, *Plasma Sources Sci Technol.*, 1996, 5, 567-572.
- (31) P.J. Bruggeman, N. Sadeghi, D.C. Schram and V. Linss, *Plasma Sources Sci. Technol.*, 2014, 23, 023001-023033.
- (32) S. Bhattacharyya, C. Cardinaud and G. Turban, *J. Appl. Phys.*, 1998, 83, 4491.
- (33) Y.H. Choi, J.H. Kim, K.H. Paek, W.T. Ju and Y.S. Hwang, *Surf. Coat. Technol.*, 2005, 193, 319–324.
- (34) H.R. Barzegar, E. Gracia-Espino, T. Sharifi, F. Nitze and T. Wågberg, *J. Phys. Chem. C*, 2013, 117, 25805–25816.
- (35) Z. Wan, R. Cai, S. Jiang and Z. Shao, *J. Mater. Chem.*, **2012**, 22, 17773- 17781.

- (36) Xue. Li, H.C. Lin, W.J. Cui, Q. Xiao and J.B. Zhao, *ACS Appl. Mater. Interfaces*, 2014, 6, 7895–7901.
- (37) L. Zhao, Y.S. Hu, H. Li, Z. Wang, L. Chen, *Adv. Mater.* 2011, 23, 1385–1388.
- (38) M.S. Song, R.H. Kim, S.W. Baek, K.S. Lee, K. Park and A. Benayad, *J. Mater. Chem. A*, 2014, 2, 631–636.
- (39) Y.B. He, M. Liu, Z.D. Huang, B. Zhang, Y. Yu, B. Li, F. Kang, J.K. Kim, *J. Power Sources*, 2013, 239, 269-276.
- (40) C. Han, D. Yang, Y. Yang, B. Jiang, Y. He, M. Wang, A.Y. Song, Y.B. He, B. Li and Z. Lin, *J. Mater. Chem. A*, 2015, 3, 13340–13349.
- (41) B. Zhang, Y. Liu, Z. Huang, S. Oh, Y. Yu, Y.W. Mai and J.K. Kim, *J. Mater. Chem.*, 2012, 22, 12133–12140.
- (42) Z. Liu, N. Zhang and K. Sun, *J. Mater. Chem.*, 2012, 22, 11688–11693.
- (43) L.G. Bulusheva, A.V. Okotrub, A.G. Kurennya, H. Zhang, H. Zhang, X. Chen and H. Song, *Carbon*, 2011, 49, 4013-4023.
- (44) A.Y. Shenouda and H.K. Liu, *J. Alloys Compd.*, 2009, 477,498- 503.
- (45) T.F. Yi, J.Z. Wu, M. Li, Y.R. Zhu, Y. Xie and R.S. Zhu, *RSC Adv.*, 2015, 5, 37367–37376
- (46) K. Wu , J. Yang, X.Y. Qiu, J.M. Xu, Q.Q. Zhang, J. Jin and Q. C. Zhuang, *Electrochim. Acta*, 2013, 108, 841-851.
- (47) N. Li, G. Zhou, F. Li, L. Wen and H.-M. Cheng, *Adv. Funct. Mater.* 2013, 23, 5429–5435.

- (48) H. Li, L. Shen, K. Yin, J. Ji, J. Wang, X. Wang and X. Zhang, *J. Mater. Chem. A*, 2013, 1, 7270-7276.

Figure Captions

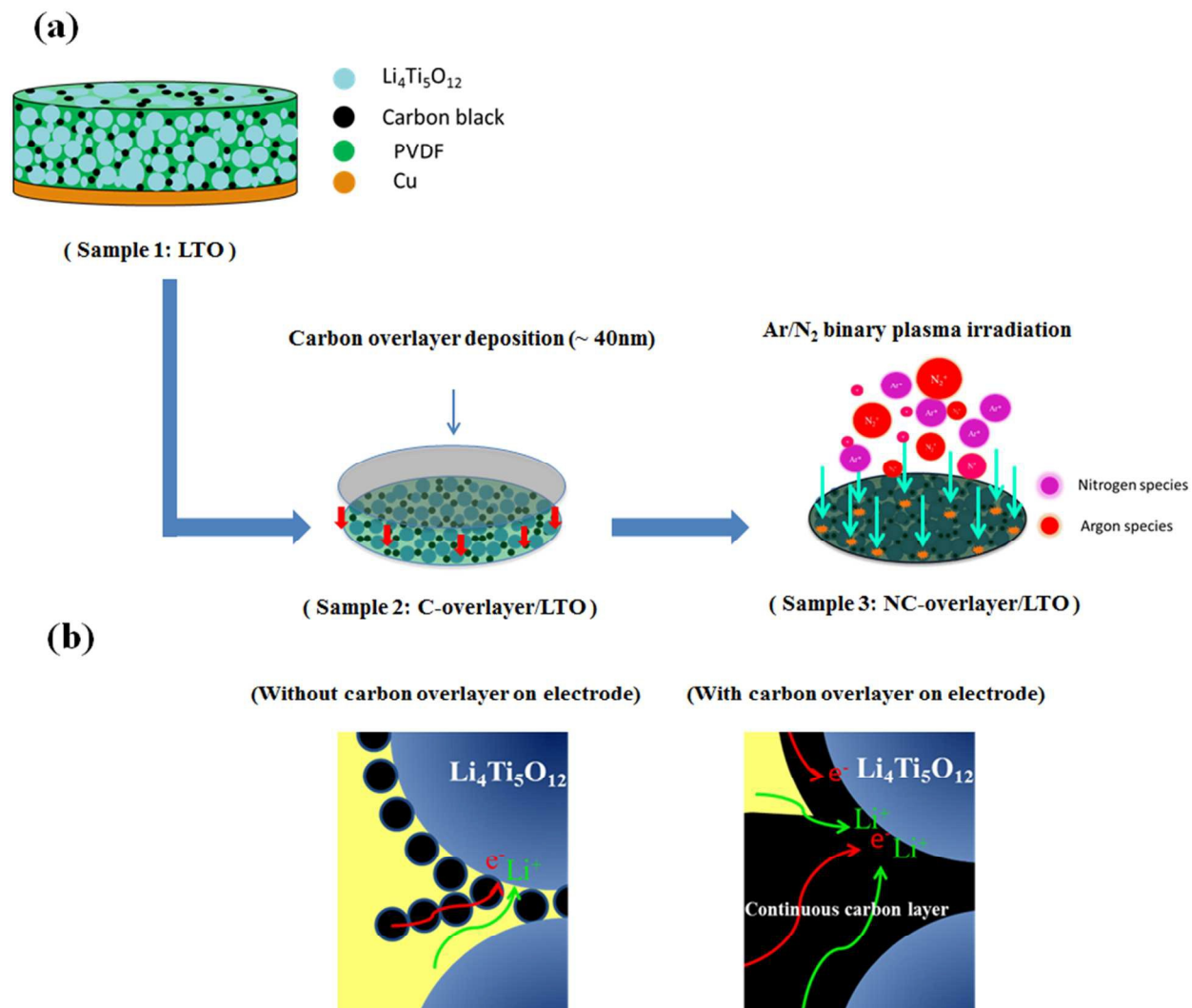


Figure 1. (a) The schematic illustration of a typical fabrication process. (b) Schematic representation of transport in $\text{Li}_4\text{Ti}_5\text{O}_{12}$ composite electrodes with and without carbon overlayer deposition.

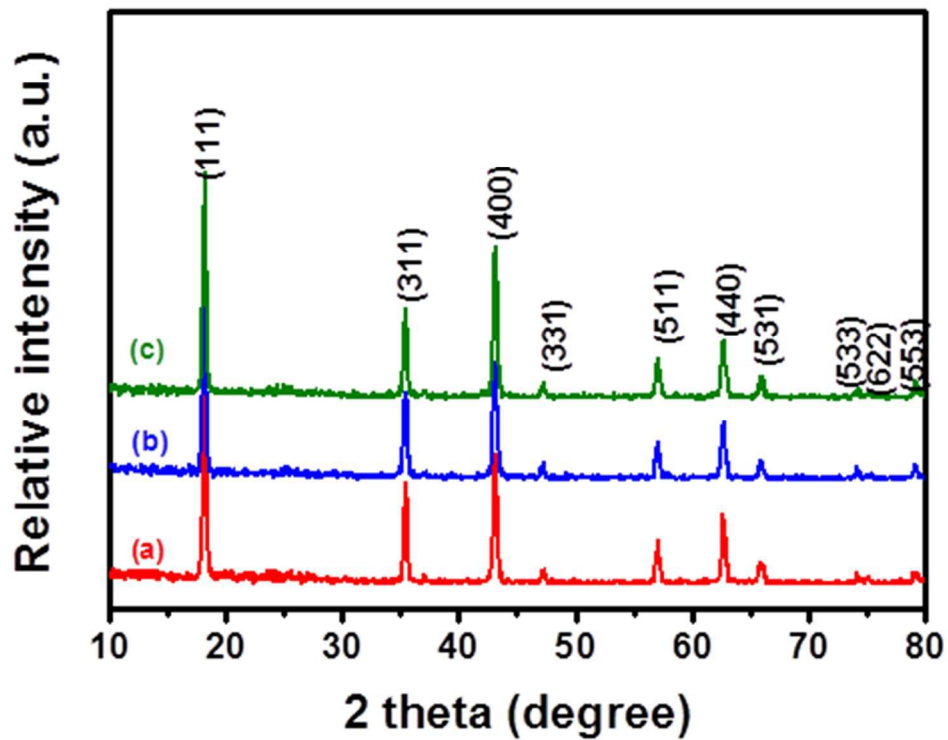


Figure 2. Comparison of grazing-incident X-ray diffraction patterns of (a) LTO, (b) C-overlayer/LTO and (c) NC-overlayer/LTO.

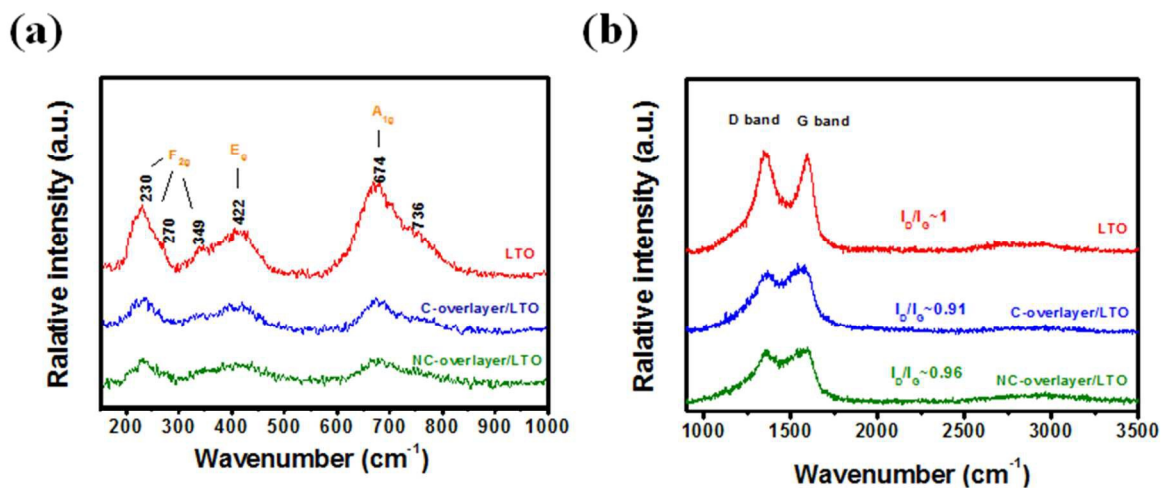


Figure 3. Raman spectrum of LTO, C-overlayer/LTO and NC-overlayer/LTO within the ranges of (a) 150-1000 and (b) 900-3500 cm^{-1} .

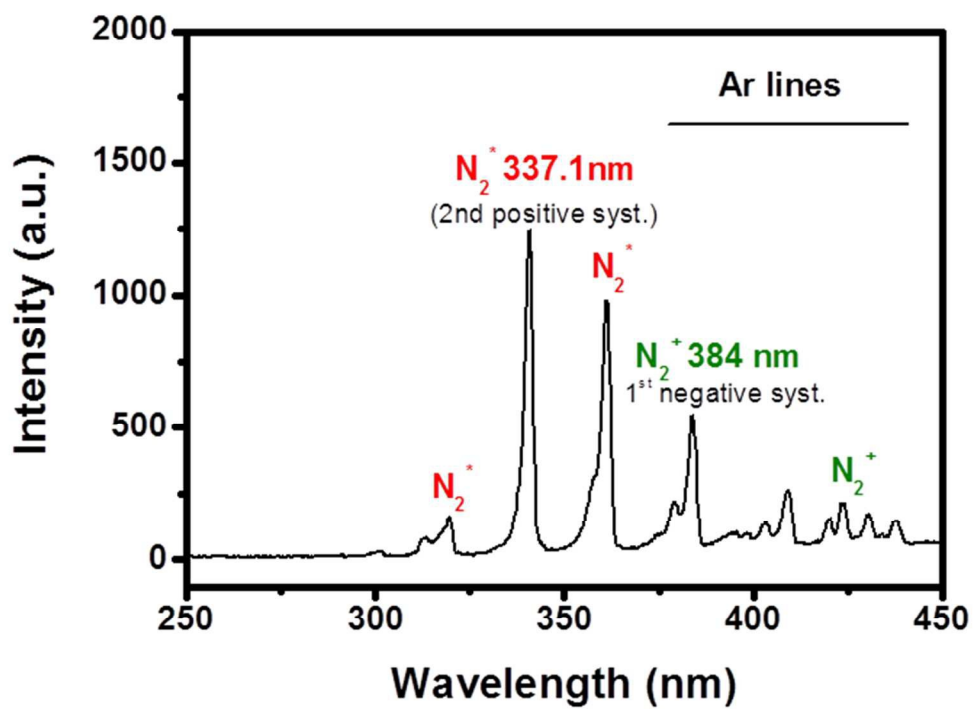


Figure 4. Principal emission lines of Ar/N₂ plasma measured by OES.

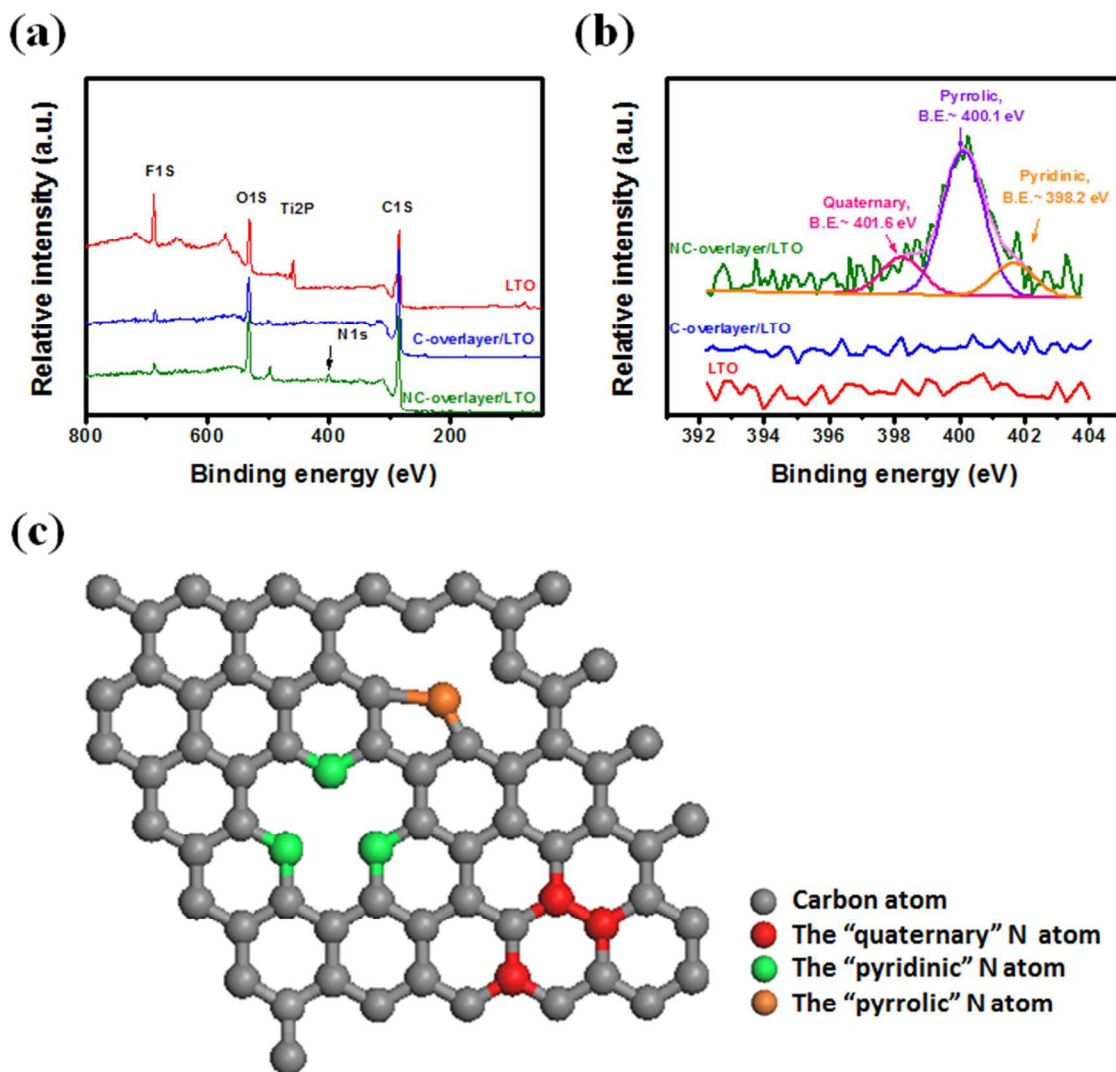


Figure 5. (a) The XPS survey spectra of LTO, C-overlayer/LTO and NC-overlayer/LTO. (b) The HR XPS spectra of Ti 2p peaks for LTO, C-overlayer/LTO and NC-overlayer/LTO. (c) Schematic illustration of nitrogen-bonding configurations in the nitrogen-doped carbon overlayer with different doping sites.

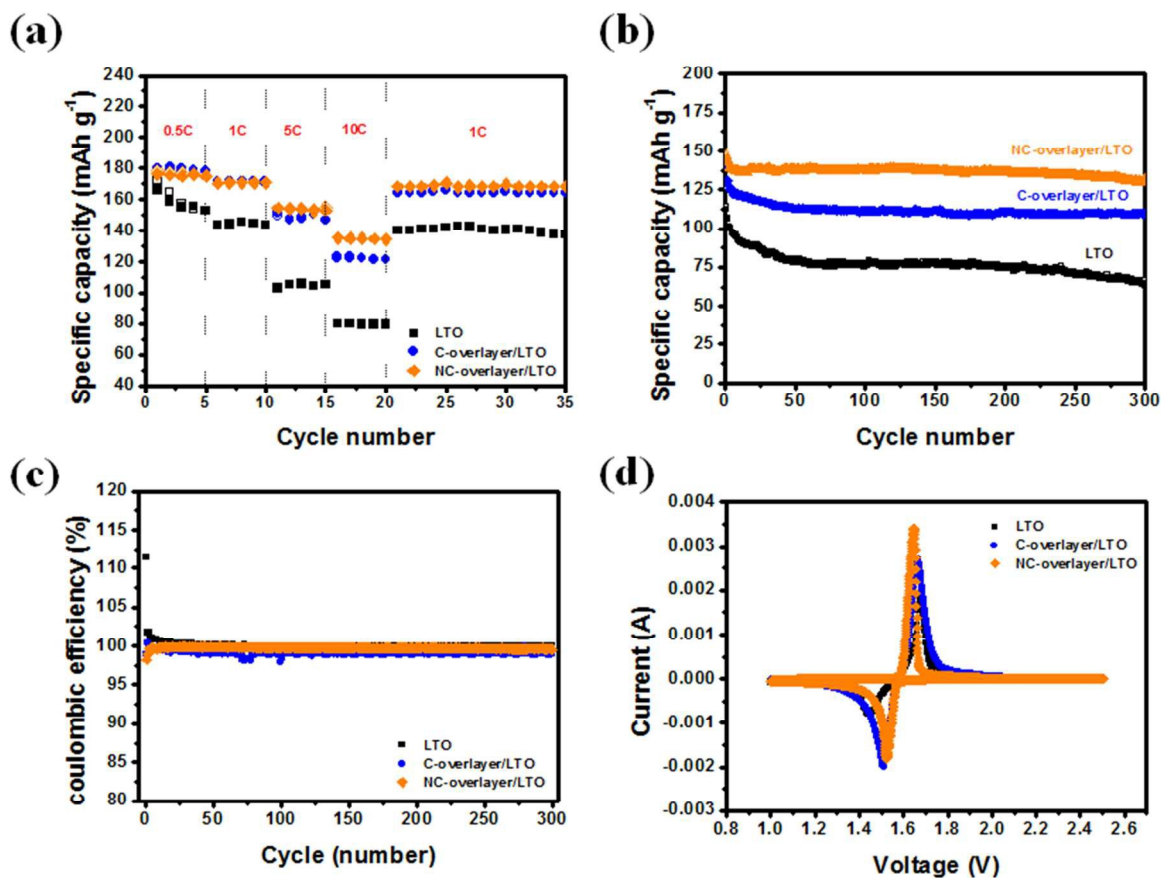


Figure 6. (a) The C rate performance of LTO, C-overlayer/LTO and NC-overlayer/LTO. (b) The cycling performance and (c) corresponding coulombic efficiency of LTO, C-overlayer/LTO and NC-overlayer/LTO at the C rate of 10C. (d) The cyclic voltammetry of LTO, C-overlayer/LTO and NC-overlayer/LTO at the scan rate of 0.1 mV/s.

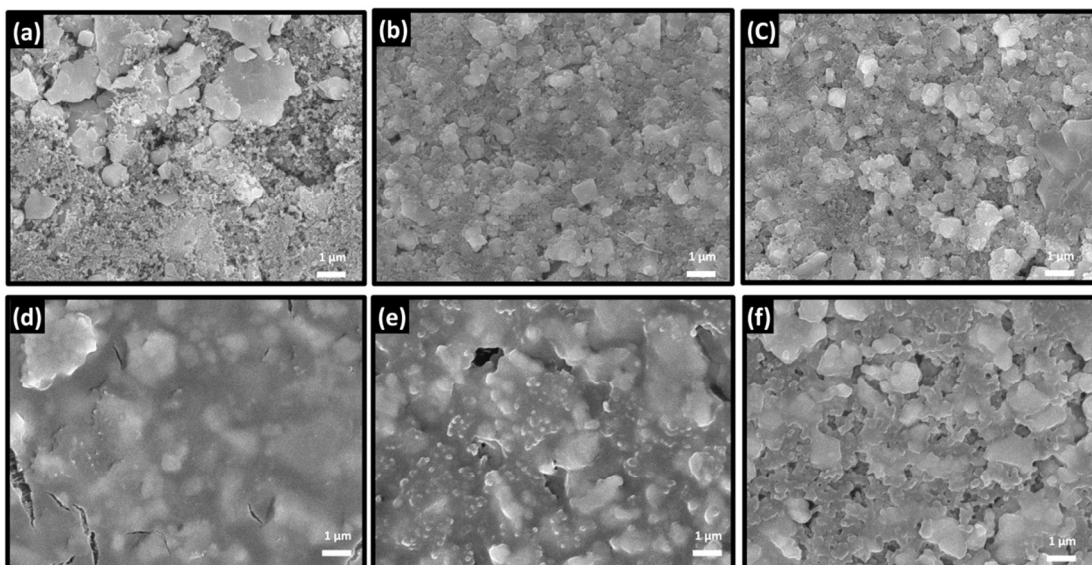


Figure 7. SEM images (top view) of (a) LTO, (b) C-overlayer/LTO and (c) NC-overlayer/LTO electrodes before cycling. SEM images of (d) LTO, (e) C-overlayer/LTO and (f) NC-overlayer/LTO electrodes after cycling at 0.1C for 10 cycles.

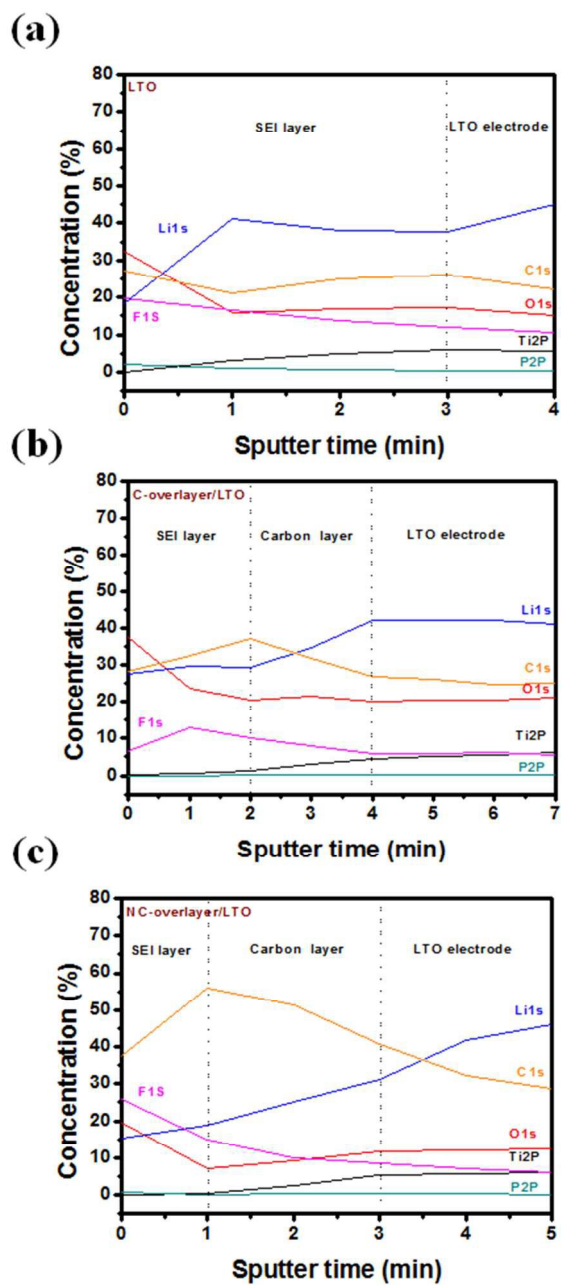


Figure 8. XPS Depth profile of (a) LTO, (b) C-overlayer/LTO and (c) NC-overlayer/LTO electrodes after cycling.

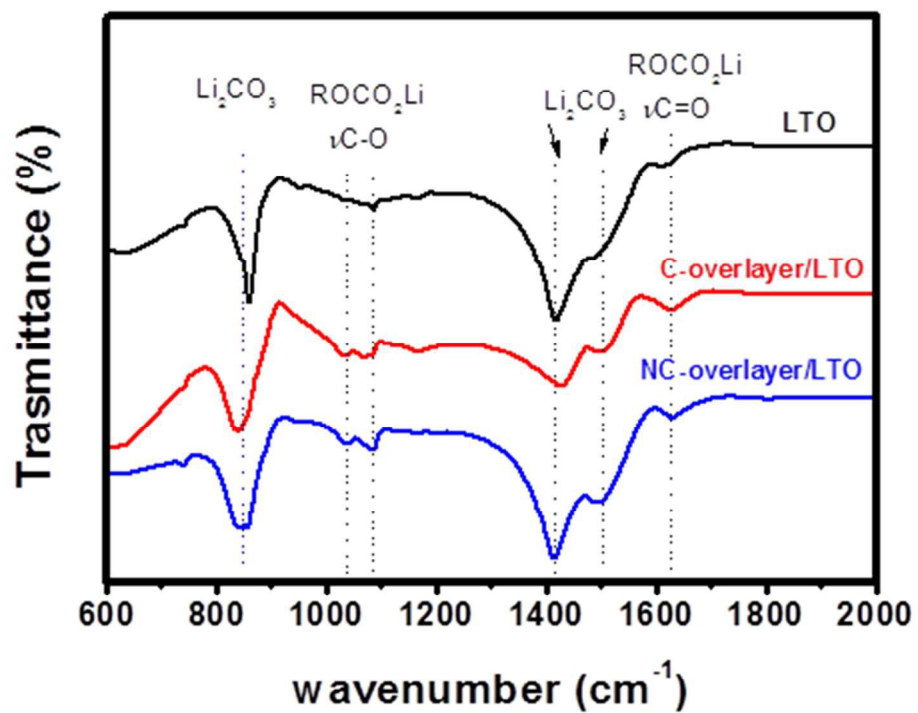


Figure 9. FTIR spectra of LTO, C-overlayer/LTO and NC-overlayer/LTO electrodes after cycling.

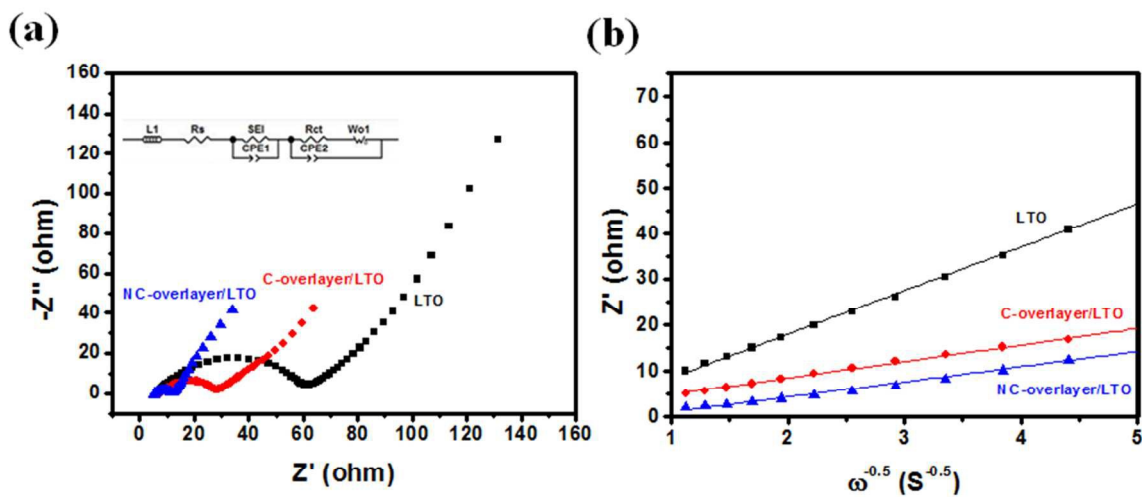


Figure 10. (a) Nyquist plots of LTO, C-overlayer/LTO and NC-overlayer/LTO. (b) The graph of Z' against $\omega^{-0.5}$ at the low frequency region.

Table 1. Parameters obtained from the cyclic voltammetry test.

Sample name	Peak _{anode} (V)	Peak _{cathode} (V)	ΔP_{ac} (mV)
LTO	1.448	1.677	229
C-overlayer/LTO	1.508	1.665	157
NC-overlayer/LTO	1.523	1.645	122

Table 2. The parameters obtained from the EIS measurement.

Sample name	R_s	R_{SEI}	R_{ct}	σ_w ($\Omega \text{ cm}^2/\text{s}^{0.5}$)	$D(\text{cm}^2/\text{s})$
LTO	6.132	27.52	25.76	9.55	1.76×10^{-9}
C-overlayer/LTO	7.231	14.59	4.991	3.59	1.25×10^{-8}
NC-overlayer/LTO	4.69	4.791	1.137	3.31	1.47×10^{-8}